

DAMTP-2001-69  
 OUTP-01-44P  
 hep-lat/0108022

August 2001

# ON THE GLUEBALL SPECTRUM IN $O(a)$ IMPROVED LATTICE QCD

UKQCD Collaboration

A. Hart<sup>a</sup> and M. Teper<sup>b</sup>

<sup>a</sup>DAMTP, CMS, University of Cambridge, Wilberforce Road,  
 Cambridge CB3 0WA, England

<sup>b</sup>Theoretical Physics, University of Oxford, 1 Keble Road,  
 Oxford OX1 3NP, England

Abstract.

We calculate the light 'glueball' mass spectrum in  $N_f = 2$  lattice QCD using a fermion action that is non-perturbatively  $O(a)$  improved. We work at lattice spacings  $a = 0.1$  fm and with quark masses that range down to about half the strange quark mass. We find the statistical errors to be moderate and under control on relatively small ensembles. We compare our mass spectrum to that of quenched QCD at the same value of  $a$ . Whilst the tensor mass is the same (within errors), the scalar mass is significantly lighter in the dynamical lattice theory, by a factor of  $0.84 \pm 0.03$ . We discuss what the observed  $m_q$  dependence of this suppression tells us about the dynamics of glueballs in QCD. We also calculate the masses of flux tubes that wind around the spatial torus, and extract the string tension from these. As we decrease the quark mass we see a small but growing vacuum expectation value for the corresponding flux tube operators. This provides clear evidence for 'string breaking' and for the (expected) breaking of the associated gauge centre symmetry by sea quarks.

PACS numbers: 12.38Gc, 12.39Mk

# 1 Introduction

The spectrum of the lightest states in the  $SU(3)$  gauge theory is by now well established (for a review see [1] and for more recent work see [2, 3]). The lightest state is a scalar ( $J^{PC} = 0^{++}$ ) with mass around  $3.6 \sqrt{K}$ , followed by a tensor ( $J^{PC} = 2^{++}$ ) at around  $5.1 \sqrt{K}$ , with  $K$  being the string tension. We may also regard this as being the glueball spectrum of the quenched approximation to QCD. In QCD the string tension is believed to have a value  $\sqrt{K} \approx 450 \text{ MeV}$ , so this means that the lightest scalar and tensor in (quenched) QCD are expected to have masses of approximately 1600 MeV and 2300 MeV respectively.

These masses have been arrived at by performing simulations for a range of lattice spacings, and then removing the discretisation effects by making an extrapolation to the continuum limit. To obtain the masses in physical MeV units involves the use of a physical scale parameter, most commonly either the string tension (e.g. in [3]) or the intermediate Sommer scale,  $r_0$  [4] (e.g. in [2]). The variations in the continuum mass estimates that arise from the use of different scale parameters are small but significant, and this highlights the inevitable uncertainties that exist in using the computationally attractive quenched approximation to describe the real world.

In the case of glueballs, the real world appears to be considerably more complicated than quenched QCD. In the mass region around 1500 MeV there are at least two and probably three flavour singlet scalar resonances. While the precise nature of these states is unclear, an attractive interpretation is that they are the result of mixing between the two flavour singlet pure qq states ('quarkonia') of the scalar nonet, and the lightest scalar glueball whose mass, as we have remarked above, should be in this mass range. The mixing models (see e.g. [5, 6]) are not sufficiently constrained, however, for any one of them to be compelling. The additional scalar states that lie below 1 GeV and which have been interpreted as diquark-antidiquark or meson-meson states complicate the picture further.

Indeed it is not clear that one should expect a simple mixing scenario to be able to explain the observed pattern of states. The presence of quarks will change the vacuum and there is no fundamental reason to think that the mass spectrum of QCD can be approximately described as consisting of the glueballs of the pure gauge theory, the usual quarkonia and, where these are close in mass, mixtures of the two. There is, of course, a constellation of observed phenomena — the OZI rule, small sea quark effects etc. — that provides some support for the simple mixing scenario. Lattice QCD calculations can help to determine whether this is indeed so. The fact that one can smoothly decrease the quark mass from large values, where the mass spectrum can be easily understood in terms of glueballs and quarkonia, down to the smaller values where the vacuum is very different from that of the pure gauge theory, provides lattice QCD with an advantage over experiment and phenomenology in determining the dynamics. (In addition lattice calculations can vary the volume and the number of colours, which can also be useful in this context.) For large quark masses the vacuum is close to that of

the pure gauge theory ('gluodynamics') and the quarkonia are heavy, so we expect that the states which are most readily visible when we use purely gluonic lattice operators similar to those used in Monte Carlo simulations of pure gauge theories, should be just the glueballs of gluodynamics. If, when we reduce the sea quark mass, the main new effect is mixing with quarkonia that are nearby in mass, we would expect that the visible states maintain their overlap onto these same operators, except in the range of quark masses where such mixing takes place. Moreover we would expect the mass to be constant except, once again, when mixing occurs. In this situation one can talk of 'glueballs' in QCD. For simplicity we will refer to states calculated in the same way as in the pure gauge theory as 'glueballs' during the remainder of this paper, although, of course, whether such language is justified is precisely one of the things we will be investigating.

Lattice QCD calculations are time consuming and this will limit the scope of our calculations. The largest lattice we can simulate is  $16^3 32$ . To maintain a large enough physical volume means that our lattice spacing cannot be significantly below  $a \approx 0.1 \text{ fm}$ . We use a non-perturbatively  $O(a)$  improved quark action, so that the lattice corrections should decrease rapidly, proportional to  $a^2$ , as we decrease  $a$ . Unfortunately the improvement coefficients are not known for  $\beta < 5.2$  and this means we cannot increase the value of  $a$  significantly beyond  $a \approx 0.1 \text{ fm}$ . Thus our calculations are limited to a narrow range of lattice spacings. This means that we are unable to say much about the continuum limit of our glueball masses. It also means that we cannot easily tell whether any difference that we observe with gluodynamics is due to lattice corrections or is a genuine physics effect. This is likely to be a particular problem for the scalar glueball (and perhaps for other  $J^{PC} = 0^{++}$  states) which, in gluodynamics at least, possesses quite large lattice corrections at this value of  $a$ . This so-called 'scalar dip' is related to a critical point in the plane of fundamental and adjoint couplings, that is close to the Wilson axis and where the scalar glueball mass vanishes, e.g. [7, 8, 9, 10, 11, 2, 12].

Another potential problem concerns the accuracy of our glueball mass calculations. Glueball (and other flavour singlet) correlation functions are notorious for their poor signal to noise ratios, which decrease rapidly with  $t$ . In gluodynamics one typically needs  $O(10^5)$  Monte Carlo sweeps in order to extract anything useful on the lightest glueball masses at  $a \approx 0.1 \text{ fm}$ . Whether one can obtain something meaningful on our modest sized dynamical QCD runs is thus far from clear.

One purpose of this paper, then, is to learn more about the statistical and systematic errors discussed above, so as to provide useful information for future lattice QCD studies. We do this by attempting to calculate glueball masses on ensembles of lattice QCD fields recently produced by the UK QCD Collaboration [13]. We find, remarkably, that even on these moderately sized ensembles, we can robustly calculate the masses of the lightest glueball excitations.

Our second purpose is to learn something about how sea quarks affect the glueball

component of the hadron spectrum, as discussed above. Here it will be important to find arguments that enable us to distinguish lattice artifacts from genuine sea quark effects.

The structure of this paper is as follows. In Section 2 we discuss the UKQCD ensembles, and the methods used for estimating the correlation functions from which we extract string tensions and glueball masses. (Details are relegated to the Appendix.) In Section 3 we present our results for the flux tubes that wind around a spatial torus ('torelons') from which we extract string tensions. We also show that these flux tubes become increasingly unstable as the quark mass is reduced – an example of 'string breaking'. In Section 4 we present our results for the glueball masses. We compare these to the quenched glueball spectrum at the same value of  $a$  and attempt to disentangle lattice and finite volume artifacts from genuine sea quark effects. Finally we summarise and discuss our results in Section 5.

For a recent study of the the glueball spectrum in the presence of sea quarks which uses an unimproved Wilson action, we refer to [14]. Recent studies of mixing can be found in [15, 16]. Results from this study for one value of the quark mass have been presented in [13], and in a much more preliminary form in [17].

## 2 Methods

### 2.1 Ensembles

In this paper we use six ensembles of SU(3) lattice gauge fields that have been recently generated by the UKQCD collaboration using a QCD lattice action with  $N_f = 2$  degenerate flavours of (dynamical) sea quarks [13]. As shown in Table 1, these ensembles (labelled  $e_n$ ) have been produced with two notable features. The first is the use of an improved action, such that leading order lattice discretisation effects are expected to depend quadratically, rather than linearly, on the lattice spacing (just as in gluodynamics). In addition, the action parameters have been chosen to maintain specific values of the lattice spacing and quark mass.

The SU(3) gauge fields are governed by the Wilson plaquette action, with 'clover' improved Wilson fermions [13]. The improvement is non-perturbative, with the coefficient  $c_{sw}$  chosen to render the leading order discretisation errors quadratic (rather than linear) in the lattice spacing,  $a$ .

The theory has two coupling constants. In pure gluodynamics the gauge coupling,  $\beta$ , controls the lattice spacing, with larger values reducing  $a$  as we move towards the critical value at  $\beta = 1$ . In simulations with dynamical fermions it has the same role for a fixed fermion coupling,  $\kappa$ . The latter controls the quark mass, with  $\kappa \rightarrow 0$  from below corresponding to the massless limit. In dynamical simulations, however, the fermion coupling also affects the lattice spacing, which will become larger as  $\kappa$  is reduced (and hence  $m_q$  increased) at fixed  $\beta$ .

Ensembles  $e_6$ ,  $e_5$  and  $e_4$  (in order of decreasing sea quark mass) have been generated with appropriately decreasing  $\beta$  as  $a$  is increased, so the couplings are ‘matched’ to maintain a constant lattice spacing, as defined by  $\hat{r}_0 = r_0/a$  [18, 19], whilst approaching the chiral limit<sup>1</sup>. This lattice spacing is ‘equivalent’ to  $a = 0.1593$  in gluodynamics with a Wilson action. Discretisation and finite volume effects should thus be of similar sizes on these lattices. Ensembles  $e_3$  and  $e_2$  are similarly matched at a slightly finer lattice spacing. In addition, ensembles  $e_3$  and  $e_4$  were chosen to have matched chirality (i.e. to have the same value of  $m_{\text{PCAC}}$  and hence of the sea quark mass) at different lattice spacings with a view to an eventual continuum extrapolation. Finally, we include results for a slightly smaller ensemble  $e_1$ , which has the lightest sea quarks at the finest lattice spacing, ‘equivalent’ to  $a = 0.1600$ . For an explicit description of the action, see [13]. An illustration of the parameter space may be found in [20]. The lattices all have a spatial extent  $L > 1.5 \text{ fm}$ , which is significantly larger than many quenched simulations, and this should ensure that any finite volume corrections are minor. (We will discuss this further below.)

Four-dimensional lattice gauge theories are scale invariant, and the dimensionless lattice quantities must be cast in physical units through the use of a known scale. That is, a specific quantity measured on the lattice (at a finite lattice spacing) is defined to agree precisely with its known physical value by multiplying by the appropriate powers of the lattice spacing. In this work we shall use (separately) two such scales; the string tension extracted from the ground state mass of ‘torelons’, single closed periodic flux tubes that wind around the periodic spatial lattice, and the Sommerer scale,  $r_0$ , extracted from potential calculations. We present here details of the determination of the former, whilst measurements of the Sommerer scale and further details of the UKQCD ensembles are described in [13].

Measurements were made on ensembles of  $N_{\text{conf}} = 280 - 830$  configurations of size  $L^3T = 16^3 32$ , separated by ten hybrid Monte Carlo trajectories. Correlations in the data were managed through ‘jack-knife binning’ of the data, using bin sizes large enough that neighbouring bin averages may be regarded as uncorrelated. In practice this amounted to dividing the data into ten bins of length between 280 and 830 trajectories. Where the Sommerer scale has been employed, its errors are combined in quadrature with those of the mass. For quantities in units of the string tension, the statistical error estimate comes from a combined ‘jack-knife bin analysis’. It is to the determination of the string tension that we turn next.

## 2.2 Torelons: calculating the string tension

In a periodic, spatial volume colour flux tubes can close upon themselves by winding around the spatial torus. If we are in the low temperature confining phase of gluodynamics such a closed loop of flux will be stable. Such a state, with unit net winding

---

<sup>1</sup>We use circumflex accents to denote dimensionless lattice quantities.

number in one of the spatial directions, is often referred to as a 'torelon'. To a first approximation the mass of such a state is the spatial extent of the lattice multiplied by the energy per unit length of the flux tube, that is the string tension. In the infinite volume limit the torelons become very massive and decouple from the observed spectrum. Including the usual universal string correction [21], we expect the torelon mass to vary with the lattice size as

$$m_t = K \hat{L} - \frac{(D-2)}{6L} : \quad (1)$$

where  $K$  is the lattice string tension and  $D$  is the dimensionality of space-time. We estimate the mass of this state by measuring correlations of spatial Polyakov loop operators

$$(n) = \text{Tr} \prod_{k=1}^3 U(n + k\hat{e}) : \quad (2)$$

for  $i = 1::3$ . These are summed in various momentum combinations up to  $P = P = 2$  in units of the lowest momentum  $\frac{2}{L}$ . We improve the overlap of the operator onto the ground state by iteratively smearing and blocking the gauge fields as described in Appendix A.1. Improvement levels  $i = 5;6$  were found to best saturate the ground state overlap (but we could include all levels in a  $7 \times 7$  correlation matrix without loss of robustness).

This simple description becomes more complicated in QCD, where colour flux tubes can break. If the decay width is small, the flux tube will still be a well-defined, albeit unstable, state. In that case we will be able to proceed with the above analysis with some modifications, as described in detail later on.

## 2.3 Calculating glueball masses

For the purposes of this paper we shall concentrate on the lightest glueball states only, as we possess neither large enough ensembles, nor small enough (timelike) lattice spacings for a comprehensive calculation of the spectrum. As a rough estimate, and by analogy with gluodynamic calculations at the same value of  $a$ , we could, at best, hope to make accurate determinations of the scalar mass (the  $A_1^{++}$  which becomes  $J^{PC} = 0^{++}$  in the continuum limit). We may also be able to obtain some estimates of the tensor ( $T_2^{++}$ ), and perhaps also the pseudoscalar ( $A_1^+$ ), the vector ( $T_1^+$ ) and the first excited state of the scalar. We will, in fact, find that while we can estimate the scalar and tensor ground state masses, we can do no more than put upper bounds on the higher states.

To calculate the mass of a glueball excitation with given quantum numbers, it is necessary to measure correlation functions of operators with the same symmetry properties (referred to as being 'in the same channel') [22], and with improved overlap onto the low-lying states of that channel. The operators at each site are summed over

all spatial sites in a timeslice to create momentum eigenstates for  $3$  momenta up to  $P_x = P_y = 2$ .

Gauge links are improved as in Appendix A.1, and we extract masses either from zero-momentum effective masses or, in the case of the light scalar, by variational analysis of a reduced,  $8 \times 8$  correlation matrix utilising momenta  $P_x = P_y = 0; 1$ . This is explained in Appendix A.2, where details of fits to individual states are given.

### 3 Torelons and the string tension

In the confining phase of gluodynamics the Polyakov loop operator shown in Eqn. 2 has zero overlap onto a contractible loop of the kind one uses as a trial glueball wave-functional. This implies that a winding flux tube has zero probability to turn into a glueball. Physically it is a consequence of the fact that the flux tube cannot break. Mathematically it is a consequence of the following symmetry argument. Suppose the Polyakov loop winds once around the  $x$ -torus. Choose some value of  $x$ , say  $x_0$ , and multiply all the link matrices in the direction  $x$  at  $x = x_0$  by  $z_i$ , a non-trivial element of the centre of the group,  $Z(3)$ , i.e.

$$U_x(x_0; y; z; t) \rightarrow z_i U_x(x_0; y; z; t) \quad \forall y; z; t: \quad (3)$$

Let the original and transformed fields be labelled  $fU_1 g$  and  $fU_1^z g$  respectively. Since the Haar integration measure  $dU_1$  and the plaquette action are invariant under the transformation in Eqn. 3, the fields  $fU_1 g$  and  $fU_1^z g$  appear with exactly the same weight in the path integral. Now in a contractible loop, such as the plaquette, any factor of  $z_i$  from a forward going link is necessarily matched by a corresponding factor of  $z_i^{-1}$  from a backward going link so the value of the loop is unchanged. By contrast,  $U_x$  will acquire just a single factor of  $z_i$ . The argument applies to any element of the centre and therefore the vacuum expectation value (VEV) of the Polyakov loop will satisfy

$$\langle U_x \rangle = \sum_{z \in Z_3} z \langle U_x \rangle = 0: \quad (4)$$

A similar calculation shows that the correlation function of a Polyakov loop with a glueball operator is also zero. This argument only breaks down if the symmetry is spontaneously broken, so that the the path integral becomes restricted to a subset of fields, and the vacuum ceases to be symmetric. This occurs, of course, at high temperature where confinement is lost, if we consider Polyakov loops,  $U_t$ , that wind around the Euclidean time torus. By the same token it will occur for a Polyakov loop that winds around the  $x$ -torus, as here, if the size of this torus is reduced below a critical value.

All the above remains true for blocked or smeared operators. For instance, on quenched  $16^4$  lattices at  $\beta = 5.93$  (where  $\hat{t}_0$  is approximately the same as on our

dynamical ensembles  $e_4, e_5$  and  $e_6$ ) we find  $\langle h \rangle = (7 \pm 13) \times 10^{-6}$ . Upon blocking the value remains consistent with zero, being  $(7 \pm 24) \times 10^{-6}$  after four blocking steps.

In QCD (always at low  $T$ ) the symmetry in Eqn. 3 is broken explicitly by the fermionic piece of the action, because the latter is linear in the link matrices. We can estimate the importance of this effect as follows. Suppose we integrate out the fermionic fields (as indeed one does in practice). The result is a partition function that is just as in the pure gauge theory except that the integrand acquires an extra factor, the determinant of the Dirac operator  $\det(D(U) + m_q)$ , for each fermion flavour. The  $\det(D(U) + m_q)$  can be expanded as a sum over closed loops and we can divide this sum into two pieces:  $\det_C$  that consists of the (contractible) closed loops that transform trivially under Eqn. 3, and  $\det_{NC}$  that consists of the (non-contractible) closed loops that transform non-trivially under Eqn. 3. The latter contains products of closed loops, one of which must wind once around the  $x$ -torus. Thus, specialising for simplicity to the case of one flavour,

$$\begin{aligned} \langle h \rangle &= \frac{1}{Z} \int \prod_{x,y} dU_{1,x} (\det_C(D(U) + m_q) + \det_{NC}(D(U) + m_q)) e^{S_G} \\ &= \frac{1}{Z} \int \prod_{x,y} dU_{1,x} \det_{NC}(D(U) + m_q) e^{S_G}; \end{aligned} \quad (5)$$

where  $S_G$  is the usual plaquette action. If the quark mass is large, the winding loop contributes  $\sim (1 - m_q)^L$  and loops are rare so that we can factorise  $\det_{NC} \sim (1 - m_q)^L \det_C$  and so we find

$$\begin{aligned} \langle h \rangle &= \frac{1}{Z} \int \prod_{x,y} dU_{1,x} \det_{NC}(D(U) + m_q) e^{S_G} \\ &\quad / \frac{1}{m_q} : \end{aligned} \quad (6)$$

The minus sign is because we have a closed fermion loop. (We have periodic spatial boundary conditions on the fermions.) All this is true not only for simple loops but also for smeared Polyakov loops. The argument extends trivially to any spatial direction and to any number of flavours.

Eqn. 6 embodies our expectation that as the sea quark mass becomes large, the quenched limit is approached and the VEV goes to zero. As the sea quark becomes lighter the VEV will, at first, rapidly increase, but at some point the mass in the winding loop will approach a value that reflects the finite constituent quark mass in the theory, and thereafter the VEV will no longer vary so rapidly.

A simple Polyakov loop can be regarded as the propagator of a heavy fundamental source and we may thus use  $\langle h \rangle / \exp(-\hat{F}L)$  to calculate a 'spatial' quark free energy. Since a non-zero value of  $\langle h \rangle$  requires a quark to propagate around the lattice, we may also use its value to determine the mass of the corresponding heavy-light system. We



are here primarily interested in the flux tube and this couples to suitably smeared Polyakov loops for which such interpretations are not useful, however, and we thus do not develop them any further here.

The above discussion justifies the usual intuitive picture of how  $\chi$  acquires a non-zero vacuum expectation value. One thinks of a  $q\bar{q}$  pair popping out of the vacuum somewhere along the flux tube, separating and thus breaking the flux tube, and finally annihilating at the boundary, at which point the flux tube has disappeared. The same process could, of course, leave us with a closed, contractible flux tube, which is a potential wave-functional for a glueball. So we might expect the amplitude for glueball-flux tube mixing to be of the same order as the vacuum expectation value. If the  $q\bar{q}$  do not annihilate round the back of the torus then we are left with a potential quarkonium state. So, to the extent that the annihilation is suppressed, we can expect the amplitude for mixing with quarkonia to be larger.

In Fig. 1 we plot the vacuum expectation value of the Polyakov loop for the representative ensembles  $e_2$  and  $e_4$ . We observe a small vacuum expectation value that is nonetheless statistically significant. Of course this assumes that we have not underestimated our statistical errors. To demonstrate this we also plot the vacuum expectation values of Polyakov loop operators with  $P = 1; 2$ . From momentum conservation we expect the VEVs of these operators to be zero, and this we see is satisfied within less than two standard deviations in all cases. This shows that our statistical error estimates are indeed reliable. We can thus claim to have obtained clear evidence of flux tube breaking by dynamical quark pair production, analogous to the string breaking that one tries to see in the static quark potential, as calculated using Wilson loops.

We note that the VEV of the simple Polyakov loop is consistent with zero and that it only becomes significant as the blocking level is increased. Since the overlap onto the lightest flux tube also increases rapidly with increasing blocking level, we interpret this as telling us that what we are seeing is the breaking of this lightest flux tube. We also note that the VEV is larger for the ensemble corresponding to the lighter value of  $m_q$ . This is what we would intuitively expect for string breaking and is consistent with eqn (6).

This last point is explored in more detail in Fig. 2. Here we plot the VEV at the  $i = 5$  blocking level versus the quark mass (using the fact that  $m_q / m^2$ ). We choose the  $i = 5$  blocking level since this has the largest overlap onto the lightest flux tube. We clearly observe an increase in the VEV as the quark mass is decreased. Indeed the quark masses at which the effect turns on rapidly is broadly consistent with the mass where the suppression of the topological susceptibility becomes significant [23, 13]. This is corroborative evidence for a significant change in the properties of the QCD vacuum generated by light sea quarks, a point to which we shall return later.

As we have already remarked, the string breaking we see, while significant, is weak. We reinforce this observation by listing in Table 3 the overlap of torelons in orthogonal

spatial directions

$$M_{\text{t}}(t) = \frac{\langle h_{\text{t}}(t) \rangle \langle h_{\text{t}}(0) \rangle}{\langle h_{\text{t}}(t) \rangle \langle h_{\text{t}}(0) \rangle} \quad (7)$$

which we see is consistent with zero. The fact that these overlaps are zero also means that nothing is to be gained by producing linear combinations that transform according to irreducible representations of the rotation group.

The above tells us that while the lightest flux tube is visibly unstable in the presence of sea quarks, and increasingly so as the quark mass decreases, its decay width, for our range of quark masses, is small. We may therefore use Eqn. 1 to interpret the torelon mass in terms of the string tension, just as we would in the quenched theory. Doing so for  $P = 0; 1$  (using a variational analysis of the connected correlation matrix, as explained in Appendix A.2) we obtain the torelon masses and string tensions listed in Table 2. We remark that these string tensions are in good agreement with those that have been obtained from Wilson loop measurements in [13].

## 4 Glueballs

The scalar glueball mass is well determined in our calculations and we list our results for it in Table 4. The tensor glueball is also quite well constrained, as we see in Table 5. These scalar and tensor masses are expressed in units of the Sommer scale and the string tension in Table 9 and Table 10 respectively. The masses of other states are listed in Tables 6, 7 and 8. The errors on the masses are clearly large, and in most cases the evidence for a plateau in the effective mass for increasing  $t$  is unsatisfactory. In the interest of completeness we give our estimates for the first excited scalar, the pseudoscalar and vector glueballs, in units of  $r_0$  and  $\sqrt{K}$ , in Table 11, but we stress that these should be regarded either as crude estimates or as upper bounds.

We shall begin by comparing our results with quenched calculations at the same value of  $a$ , so as to establish what, if any, are the effects of the sea quarks. We shall then ask whether the observed effects might not be due to finite volume effects, in particular to those which are only present once we have sea quarks. We shall see that such effects can be excluded. We then discuss the implications of what we find for glueball masses in QCD.

### 4.1 Quenched comparison

To identify what effect the sea quarks have on our calculated glueball masses, we will now compare our results to those obtained in the pure gauge theory. Since our lattice spacing is quite coarse, we can expect lattice spacing corrections to be significant, and so we will make the comparison at the same value of  $a$ .

Since we are comparing two different theories, there is, strictly speaking, no such thing as the 'same' value of  $a$ . We shall, however, follow usual practice and use the

Sommer scale,  $r_0$ , to calibrate the lattice spacing. That is to say, we calculate  $r_0=a$  in the theory with and without quarks and say that  $a$  is the same when  $r_0=a$  is the same. That this is sensible is based on arguments that  $r_0$  should be insensitive to the presence of sea quarks.

Although, in principle,  $r_0$  provides a useful scale, the fact that it is extracted from the static potential at intermediate distances (around 0.5 fm) means that different ways of calculating it will differ substantially when  $a$  is coarse. This would not matter if a fixed calculational procedure were adhered to, but in practice different groups use different methods. Although this is all done in the worthy spirit of producing ‘better’ estimates of  $r_0=a$ , in practice this undermines the usefulness of  $r_0=a$  as a scale to use in comparing different calculations. In our context, this means that the only quenched calculation with which we can directly compare is the one at  $\beta = 5.93$  where  $r_0=a = 4.714(13)$  [13] using exactly the same procedures as for the QCD calculations [13]. As we see from Table 1, this lattice spacing is the same (within errors) as the one for the ensembles  $e_4$ ,  $e_5$  and  $e_6$ . The lightest glueball masses and the string tension have been calculated on a  $16^4$  lattice at  $\beta = 5.93$  in [3]. The value of the string tension obtained there is  $\hat{K} = 0.2430(23)$  which agrees well with the values we obtain on the  $e_4$ ,  $e_5$  and  $e_6$  ensembles, as quoted in Table 2. The values of  $a$  are slightly smaller on the other ensembles, with the smallest being on the  $e_1$  ensemble. If we scale up the quenched scale by the same amount (using the string tension, which should be a reliable procedure over this small range of scales) we conclude that the equivalent quenched  $a$  to the  $e_1$  ensemble is at  $\beta' = 6.0$ . Quenched calculations at this value of  $\beta$ , on a  $16^4$  lattice, have been performed and can be found in [3]. In the quenched theory, at  $\beta = 5.93$ , the lightest scalar and tensor glueball masses are  $\hat{m}_G = 3.68(8)$  and  $\hat{m}_G = 5.82(14)$  respectively. At  $\beta = 6.0$  the corresponding values are  $\hat{m}_G = 3.83(8)$  and  $\hat{m}_G = 5.90(14)$ . (The  $\beta = 6.0$  value of  $\hat{m}_G$  has been estimated by scaling the  $\beta = 5.93$  value by the ratio of the calculated string tensions.) That is to say, the tensor mass is unchanged, while the scalar increases slightly as  $\beta$  increases. We shall thus take the  $\beta = 5.93$  masses to represent the equivalent quenched values for all our six QCD ensembles.

In Fig. 3 we plot our calculated values of the lightest scalar and tensor glueball masses as a function of the square of the pion mass, which should be approximately proportional to the sea quark mass. We also plot the equivalent quenched masses (obtained at  $\beta = 5.93$  [3]) and, in addition, their continuum extrapolation [2]. We observe that the scalar mass is systematically lighter than its quenched value. If we average over the six ensembles we obtain 0.85(3) for the ratio of the dynamical to quenched scalar masses. For the tensor the corresponding ratio is 0.98(4) and here we conclude that there is no sea quark effect visible within the (not so small) errors.

Our mass estimates for the lightest pseudoscalar, the first excited scalar, and the vector have very large errors making any comparison not very significant. Nonetheless we note that the values listed in Table 11 are broadly consistent with the continuum

quenched values obtained in [2].

## 4.2 Finite volume effects

As we have just seen, our scalar glueball is significantly lighter than it is in gluodynamics at the same value of  $a$ . Before dwelling upon the implications of this observation it is important to establish that this effect is not a mere finite volume effect.

In gluodynamics, sizeable finite volume corrections first arise when the spatial volume decreases to the point where the mass of a (conjugate) pair of winding flux tubes becomes less than the value of the glueball mass on large volumes. In the first part of this Section we shall demonstrate that this effect is not significant for the scalar glueball on the  $L^3 \times \beta_0$  lattices considered here.

In the presence of sea quarks the flux tube can break and this makes it possible for the glueball to mix with a single winding flux tube. This could, potentially, introduce finite volume corrections on larger volumes. We shall examine this mechanism and show that it is negligible in the present calculation.

### 4.2.1 Mixing with torelon pairs

In the pure gauge theory the onset, as we decrease the volume, of sizeable finite volume effects, comes from mixing between glueball states and 'torelon pairs'. These are combinations of two flux tubes with net zero winding number. An example of a scalar torelon pair operator is  $T(t) = T_1(t) + T_2(t) + T_3(t)$ , where

$$T(t; P = 0) = (t; P = 0)^Y (t; P = 0): \quad (8)$$

(No sum over indices is implied and vacuum subtraction is understood.) It is clear that in a large volume the mass of this state should be close to twice the torelon energy, and proportional to the spatial extent of the lattice. When the volume is small enough, the mass of such a torelon pair becomes first comparable to and then less than the (large volume) glueball mass. It then effectively becomes the lightest glueball state (for an analysis in  $d = 2 + 1$ , see [24]). On our lattices, however, a single torelon is already slightly heavier than the scalar glueball, so the torelon pair is likely to be about twice as heavy. Thus any mixing with the scalar will be heavily suppressed and the mass itself would be expected to be too heavy to be visible in our calculations. Given the high mass, it seems unlikely that any of the glueball states that we consider will suffer finite volume effects from such torelon pairs.

### 4.2.2 Mixing with single torelons

Mixing between the scalar glueball and the torelon pair is suppressed, in our calculation, by the large mass difference between the states. As we have seen, the presence of sea quarks in the simulation breaks the centre symmetry, albeit weakly at the quark masses

accessible to us in this study. It is now possible for mixing to occur between single torelons and glueballs [25]. The torelons are, for a fixed lattice size, much lighter than the torelon pairs and this can lead to enhanced mixing and finite volume effects in dynamical simulations. A measure of the strength of the mixing is the normalised cross correlation of the ‘best’ scalar with the ‘best’ winding  $A_1^{++}$  operator:

$$M_{\text{mix}}(t) = \frac{\langle h(t) \phi(0) \rangle}{\langle h(t) \phi(0) \rangle \langle h(t) \phi(0) \rangle} : \quad (9)$$

The measurements for  $t = 0$  are tabulated in Table 3, and are clearly very small, and indeed consistent with zero. (As remarked earlier, the fact that orthogonal torelons have zero overlap, within errors, means that nothing was gained by using in Eqn. 9 the scalar sum of the three orthogonal torelons.) Thus single torelons will not lead to any significant finite size corrections to our scalar glueball masses.

### 4.3 Glueballs with sea quarks

Now that we have established that the observed suppression of the scalar glueball mass is not a finite volume effect, we can turn to a detailed discussion of its dynamical implications.

The first and rather striking feature of the scalar mass suppression, as displayed in Fig. 3, is that it appears to be independent of the quark mass. This is puzzling because our range of quark masses goes well above twice the strange quark mass where any quarkonia are expected to be much heavier than the scalar glueball and so any mixing effects should be very small. As for the vacuum, we know from our calculations of the topological susceptibility that sea quarks only become important about mid-way along the plot, where  $\hat{\rho}_0 m^2 \approx 2$  [23]. (We also see this in Fig. 2 for the torelon VEV.) Thus it would seem difficult to argue that this mass suppression is a dynamical effect due to ‘light’ quarks.

The only sizeable effects that one would expect to depend weakly on the quark mass are lattice artifacts. One can indeed make a plausible argument for this in the present case. As we have previously remarked, at this value of  $a$  the scalar mass is already suppressed in gluodynamics by the presence of a nearby critical point in the space of fundamental and adjoint couplings. If the effect of our fermionic action is effectively to add a positive adjoint piece to the pure gauge action, then this could strongly enhance the suppression, just as we observe. In fact one can show [26] that the clover term, inserted to provide the  $O(a)$  improvement, has precisely this effect. We believe this to be the most likely explanation for the suppression of the scalar glueball mass.

If this suppression is a lattice artifact, then it should disappear as we take the continuum limit. Our range of  $a$  is very limited of course, but our lever arm is enhanced by the fact that the leading corrections, with our action, are  $O(a^2)$ . Using the fact that the glueball mass appears not to depend on the quark mass, we plot all our scalar

glueball masses against  $a^2$ , in Fig. 4. We might, very optimistically, claim to see some hint here that the suppression decreases with  $a$ .

Let us assume, as argued above, that the suppression at large quark masses is a lattice artifact. Such a lattice artifact will be largely independent of the quark mass and so, if we correct the scalar glueball mass for it, we will obtain a scalar mass that does not vary significantly with  $m_q$ . In particular there will be no change at  $\hat{m} \approx 2$  where we have observed the onset of large light-quark effects in quantities such as the topological susceptibility. Thus we conclude that the scalar glueball is not sensitive to the increasing presence of quark loops in the vacuum as these become lighter. That is to say, the glueball remains a glueball.

Finally, what of mixing with quarkonia? We do not have much information on the masses of flavour singlet quarkonia for our ensembles. What we do have is the mass of two pions (in an s-wave), however. The threshold mass is just  $2m_\pi$  and this is plotted in Fig. 3. We see that this state is almost degenerate with the scalar glueball from the  $e_2$  ensemble. The fact that the mass shows no shift suggests little coupling between these states. This would be consistent with a weak mixing picture of the kind that has usually been assumed in phenomenological analyses, such as [5, 6].

All these observations are supported by the fact that our best glueball operator does not vary significantly with  $m_q$  and neither does the overlap of the lightest scalar state on this operator. This suggests that the nature of the glueball wave-functional is insensitive to the quark mass.

## 5 Conclusions

One aspect of our analysis that was a (pleasant) surprise was the relatively small statistical errors that we achieved even with our lightest quark masses. As an example we show in Table 12 how the scalar glueball effective mass, and its statistical error, compares with what one obtains in the quenched calculation. (The latter on a  $16^4$  rather than a  $16^3 32$  lattice.) We recall that the QCD calculation makes measurements every tenth trajectory in a run that totals 8300 HMC trajectories, while the quenched calculation makes measurements every fifth of  $10^5$  Monte Carlo sweeps. The difference in the errors is surprisingly modest and makes us optimistic about future QCD calculations of flavour singlet hadron masses.

We calculated the masses of what we hoped would turn out to be flux tubes winding around the spatial torus. We found that such flux tubes are indeed unstable, as one would expect in QCD, but this effect is weak enough for us to obtain accurate values of the string tension, which agree with the values obtained in the pure gauge theory with the same value of the lattice spacing. The instability of the flux tube is signalled by a non-zero vacuum expectation value of the best flux tube wave-functional, whose onset becomes marked around the strange quark mass. This may be viewed as a direct example of the expected ‘string-breaking’.

In our glueball mass calculations we found that we could obtain reliable results for the lightest scalar and tensor glueballs. The tensor mass shows no dependence on the quark mass and its value,  $\hat{r}_0\hat{m}_G = 6.0(5)$ , is consistent with what one finds in the pure gauge theory at the same value of  $a$ , i.e.  $\hat{r}_0\hat{m}_G = 5.82(14)$ . The scalar mass also shows no quark mass dependence but its value,  $\hat{r}_0\hat{m}_G = 3.0(2)$ , is significantly suppressed compared to the pure gauge theory value of  $\hat{r}_0\hat{m}_G = 3.68(8)$ . We argued that the quark mass independence of this suppression, even at quark masses as large as  $m_q = 2m_s$ , suggests that this is a lattice artifact rather than an effect due to ‘light’ quarks. This is made plausible by the observation [26], that the large clover term in our improved action, pushes the effective gauge action closer to the nearby critical point in the space of fundamental and adjoint couplings, and thus strongly enhances the  $O(a^2)$  lattice corrections. A similarly low scalar glueball mass has been seen also been seen at coarser lattice spacings for the clover action [16].

Assuming this explanation to be correct leaves no room for any significant variation of the scalar mass from its quenched value as the sea quarks become important in the vacuum. (We infer from the behaviour of the topological susceptibility and the flux tube vacuum expectation value that this occurs at about  $\hat{r}_0\hat{m} = 2$ .) This suggests that the nature of the glueball suffers no major change as light sea quarks ‘switch on’. It also leaves no room for any significant variation at the lightest quark masses where the two pion s-wave state becomes slightly lighter than the scalar glueball and where any strong coupling would presumably lead to a visible mass shift. This suggests the coupling is weak. All this fits in with the usual naive picture of the fate of glueballs in QCD: they are largely unaffected by the light quarks in the vacuum and mix weakly with quarkonia, so that only nearby quarkonia are important.

It is, of course, the case that we have read a great deal into a relatively limited set of calculations and so the above analysis should be regarded as setting a framework for future discussion, rather than being in any way definitive.

## Acknowledgements

This work was performed under the British PPARC research and travel grants to the UK QCD Collaboration. We thank D. Hepburn and D. Pleiter for preliminary estimates of pseudoscalar meson masses. A.H. acknowledges the support of PPARC grants for postdoctoral support.

## A Computational procedures

In this appendix we give details of the procedures used to obtain our mass estimates.

### A.1 Improvement of operators

To reduce statistical errors on mass estimates, it is necessary to ensure that operators have a good overlap onto the ground state excitation with the specified quantum numbers. This was achieved by a combination of smearing and blocking of the spatial links only.

Smearing [27] is computationally cheap, and does not reduce the size of the effective lattice. The smeared link is a combination of the original link and the (spatial) staples surrounding it.

$$\begin{aligned} U(n) \rightarrow U^0(n) = & c_{\text{sm}} U(n) \\ & + \sum_{\mu=1:3} U(n) U(n+\hat{\mu}) U^\dagger(n+\hat{\mu}) \\ & + U^\dagger(n-\hat{\mu}) U(n-\hat{\mu}) U(n+\hat{\mu}-\hat{\mu}) \end{aligned} \quad (10)$$

where  $c_{\text{sm}}$  is a free parameter. The smeared link is then projected back onto the gauge group.

Whilst smearing alone will couple well to the spherically symmetric scalar glueball ground state, for the tensor and torelon we find it important to include blocking steps [28] in the improvement schedule, where we increase the effective lattice spacing by a factor of two, and replace each spatial link by

$$\begin{aligned} U(n) \rightarrow U^0(n) = & c_{\text{b1}} U(n) U(n+\hat{\mu}) \\ & + \sum_{\mu=1:3} U(n) U(n+\hat{\mu}) U(n+\hat{\mu}+\hat{\mu}) U^\dagger(n+2\hat{\mu}) \\ & + U^\dagger(n-\hat{\mu}) U(n-\hat{\mu}) U(n+\hat{\mu}-\hat{\mu}) U(n+2\hat{\mu}-\hat{\mu}) \end{aligned} \quad (11)$$

where again  $c_{\text{b1}}$  is a free parameter and the blocked link is projected back onto the gauge group using a link-wise cooling procedure. Over-applying this can lead to the creation of supposedly local objects that in fact have a winding round the lattice, which we avoid.

We choose  $c_{\text{sm}} = 1.0$ ,  $c_{\text{b1}} = 1.0$  and up to six levels of iterated improvement are applied to the links, alternately smearing and blocking (beginning with the former). We label these sequentially  $i = 1:6$ , with  $i = 0$  being the original links.

### A.2 Extraction of mass estimates

Using the suite of operators, we form for each momentum channel a matrix of (vacuum subtracted) correlators  $C_{jk}(t) = \langle h_j(t) h_k^\dagger(0) \rangle$ , normalised such that the diagonal ele-



ments are unity at  $t = 0$ . From the diagonal elements we derive the effective masses, all tending to the ground state for large  $t$ ,

$$m_k^e(t) = -\ln \frac{C_{kk}(t+1)}{C_{kk}(t)} \quad (12)$$

and the overlap of the state onto the ground state

$$b_k = \frac{C_{kk}(1)^2}{C_{kk}(2)} - 1 \quad (13)$$

Most of the states we attempt to study are massive enough that the correlation functions decay rapidly into the noise. For such states we derive the mass estimate from the plateau in  $t$  of the operator that best couples to the ground state (i.e. which maximises  $b_k$  and minimises  $m_k^e(t=1; P=0)$ ).

The lightest states permit a refined estimate of the low lying masses via a variational analysis on the correlation matrix [29, 16] (see [30] for precise details of our method). For the torelon we have a  $7 \times 7$ , whilst for the scalar glueball we create a reduced  $8 \times 8$  matrix, using the four basic operators at optimal improvement levels  $i = 3; 4$ . We have also checked that reducing the basis even further, to the best two states or to simply the diagonal elements of the correlation matrix gives consistent ground state determinations.

The generalised eigenvalue problem is solved at each momentum value for the  $f = 1::N$  right eigenstates

$$\sum_{k \neq n} C_{jk}^y(t_0) C_{km}(t) v_m^{(f)}(t; t_0) = v_j^{(f)}(t; t_0) v_j^{(f)}(t; t_0) : \quad (14)$$

where  $t_0 = 0$  in all cases here. In common with most implementations, we calculate the eigenvectors with normalisation

$$\sum_{k \neq n} v_k^{(f)}(t; t_0) C_{km}(t_0) v_m^{(f)}(t; t_0) = 1 \quad (15)$$

at  $t = t_1$  and freeze them at all subsequent times. This improves the stability of the effective mass estimates. The results presented here are for  $t_1 = 1$  (in lattice spacing units), but we have checked for  $t_1 = 2; 3$  that any biases introduced are within the statistical errors. We can approximate the eigenstates of the Hamiltonian by  $v_k^{(f)}(t) = \sum_{k \neq n} v_k^{(f)}(t_1; t_0) C_{km}(t) v_m^{(f)}(t_1; t_0)$ , which satisfy  $v^{(f)} v^{(f)} = 1$ . Ground and excited state mass estimates are extracted from effective energies formed from the correlators

$$D^{(f)}(t) = \langle h^{(f)}(t) v^{(f)}(0) \rangle = \sum_{k \neq n} v_k^{(f)}(t_1; t_0) C_{km}(t) v_m^{(f)}(t_1; t_0) \quad (16)$$

In some cases we shall be interested in the overlap of our ground state eigenfunctions onto the basis operators. This is given by  $\langle h^{(f)} \rangle = \sum_j C_{kj}(t_0) v_j^{(f)}(t_1; t_0)$  (which are the left eigenvectors).

### A.3 Non{zero momentum

We can further improve the mass estimates of the lighter states by including correlators of non{zero momentum in our analysis. The lowest such is  $\frac{2}{L}$ , and in these units we measure  $P = P = 0;1;2$ . We convert these effective energies to masses using the lattice dispersion relation

$$\hat{E}^e(t;P)^2 = \hat{m}^e(t;P)^2 + \sum_{x=1}^3 \sin^2 \frac{2\pi P x}{L} : \quad (17)$$

(This form was found to be more successful than the continuum version in describing the massless photon dispersion relation in a lattice Higgs model [31].)

An immediate concern, however, is that boosting zero momentum irreps of the cubic group can mix previously orthogonal states. This can result in contamination of correlation functions by lighter states. This contamination will increase with the size of the boost and will particularly involve the lightest, scalar state.

One method of dealing with this is to explicitly subtract off the scalar contribution. We may determine this by measuring explicitly the overlap between the operator in question and the boosted scalar state. Linear combinations of the operators can then render the basis orthogonal to the scalar contamination. We may get around the problem more simply, but with the penalty of losing some information and self{averaging. Consider the continuum notation. We construct operators with a well defined eigenvalue of a component of  $J$ , rather than of  $J$  itself. We do this by building a glueball operator with chosen symmetry under rotation about a particular lattice axis. We then boost this operator, but only along this axis which does not change the angular momentum about this axis. We create, in effect, an eigenstate of helicity. This operator will then couple to the lightest state with  $J$  commensurate to this. For example, if we arrange for the glueball operator to change by a factor of  $-1$  under a rotation of  $\frac{\pi}{2}$  about the  $z$ {axis, then we  $x J_z = 2$ . The operator boosted along the  $z$ {axis can thus couple only to states with  $J = J_z$ , which was unaffected by the boost and which excludes the scalar contamination. The ground state will now be expected to be purely  $J = 2$ .

In practice, however, the contamination is easy to identify as a reduction in the effective mass plateaux of the original, boosted operators. The zero momentum correlation functions and all scalar states remain, of course, unmixed by the momentum. The  $T_2^{++}$  tensor appears unaffected for  $P = P = 1$ , but does show a reduction for  $P = P = 2$  and we exclude the latter from the mass analysis. The  $E^{++}$  shows a reduction for both non{zero momenta, and for technical reasons we do not consider this state in this work. Any possible contamination of higher mass states is within the large statistical errors of these states.

We perform joint fits to the effective mass functions obtained after variational analysis of correlation matrices and subtraction of the boost momentum. For a given state

at large  $t$ , the masses from differing momenta should become consistent with a single plateau, which gives the rest mass. The signal from the  $P = 1$  channel was found to be particularly useful. The mass of the ground state excitation were still small enough for reliable effective energy plateaux to be observed for the lighter rest mass states, and statistical noise was observed to be only of a similar magnitude to the  $P = 0$  channel. For  $P = 2$ , however, the energies of the states were often too large to be confidently assessed. Where extractable, the  $P = 2$  correlators showed a consistent effective mass plateau with lower momentum channels, bar the boost contamination discussed above. As they did not improve the quality of the fits, however, we estimate the ground state scalar mass by performing joint plateau fits to  $P = 0; 1$  uncorrelated in both  $t$  and  $P$ , over as wide a range of  $t$  as the quality of fit indicators<sup>2</sup> per degree of freedom and  $Q$  permitted. We give examples of effective mass plots for the tensor state, the heavier 1<sup>st</sup> excited scalar, the pseudoscalar and vector states in Figs. 8{10. Details of the fits made are shown in Tables 6{8, where an italic font indicates no masses were extractable beyond  $t = 1$ .

## References

- [1] M. Teper, Oxford preprint OUTP-98-88P [hep-th/9812187].
- [2] C. Morningstar and M. Peardon, Phys. Rev. D 60 (1999) 034509 [hep-lat/9901004].
- [3] B. Lucini and M. Teper, JHEP 0106 (2001) 050 [hep-lat/0103027].
- [4] R. Sommer, Nucl. Phys. B 411 (1994) 839 [hep-lat/9310022].
- [5] W. Lee and D. Weingarten, Phys. Rev. D 61 (2000) 014015 [hep-lat/9910008].
- [6] F. Close and A. Kirk, hep-ph/0103173.
- [7] G. Bhanot and M. Creutz, Phys. Rev. D 24 (1981) 3212.  
M. Creutz, Quarks, gluons and lattices (CUP, 1983).
- [8] A. Patelet al., Phys. Rev. Lett. 57 (1986) 1288.
- [9] U. Heller, Phys. Lett. B 362 (1995) 123 [hep-lat/9508009].
- [10] U. Heller, Nucl. Phys. B (Proc. Suppl.) 47 (1996) 262 [hep-lat/9509010].
- [11] C. Morningstar and M. Peardon, Nucl. Phys. (Proc. Suppl.) 73 (1999) 927 [hep-lat/9808045].
- [12] C. Morningstar and M. Peardon, Nucl. Phys. (Proc. Suppl.) 83 (2000) 887-889 [hep-lat/9911003].

- [13] [UKQCD Collaboration] C. Allton et al., hep-lat/0107021.
- [14] [SESAM-TL Collaborations] G. Bali et al., Phys. Rev. D 62 (2000) 054503 [hep-lat/0003012].
- [15] D. Toussaint, Nucl. Phys. (Proc. Suppl.) 83-84 (2000) 151 [hep-lat/9909088].
- [16] [UKQCD Collaboration] C. Michael, M. Foster and C. M. d'Neile, Nucl. Phys. (Proc. Suppl.) 83-84 (2000) 185 [hep-lat/9909036]; C. M. d'Neile and C. Michael, Phys. Rev. D 63 (2001) 114503 [hep-lat/0010019]; A. Hart, C. M. d'Neile, C. Michael and M. Teper, in progress.
- [17] [UKQCD Collaboration] A. Irving, Proceedings of Lattice 00 conference, hep-lat/0010012
- [18] [UKQCD Collaboration] A. Irving et al., Phys. Rev. D 58 (1998) 114504 [hep-lat/9807015].
- [19] [UKQCD Collaboration] J. Gaden, Nucl. Phys. B (Proc. Suppl.) 83 (2000) 165 [hep-lat/9909066].
- [20] [UKQCD-QCD SF Collaborations] S. Booth et al., hep-lat/0103023.
- [21] Ph. de Forcrand, G. Schierholz, H. Schneider and M. Teper, Phys. Lett. B 160 (1985) 137.
- [22] C. Michael, Acta Phys. Pol. B 21 (1990) 119.
- [23] [UKQCD Collaboration] A. Hart and M. Teper, Nucl. Phys. B (Proc. Suppl.) 83-84 (2000) 476 [hep-lat/9909072]; Edinburgh preprint 2000/11 [hep-ph/0004180]; hep-lat/0009008; Cambridge DAMTP preprint 2001-70 [hep-lat/0108006].
- [24] M. Teper, Phys. Rev. D 59 (1999) 014512 [hep-th/9804008].
- [25] J. Kripfganz and C. Michael, Nucl. Phys. B 314 (1989) 25.
- [26] [UKQCD Collaboration] A. Hart, Cambridge preprint DAMTP-2001-75 [hep-lat/0108nnn].
- [27] [APE Collaboration] M. Albanese et al., Phys. Lett. B 192 (1987) 163.
- [28] M. Teper, Phys. Lett. B 187 (1987) 345.
- [29] M. Luscher and U. Wol, Nucl. Phys. B 339 (1990) 222.
- [30] A. Hart, O. Philipsen, Nucl. Phys. B 572 (2000) 243 [hep-lat/9908041]; A. Hart, M. Laine, O. Philipsen, Nucl. Phys. B 586 (2000) 443 [hep-ph/0004060].
- [31] A. Hart, O. Philipsen, unpublished.

label			$c_{sw}$	$N_{\text{traj.}}$	$\hat{r}_0$	$\hat{m} = \hat{m}$	$\hat{r}_0 \hat{m}$
$e_1$	5.20	0.13565	2.0171	2800	5.21 (5)		1.386 (63)
$e_2$	5.20	0.13550	2.0171	8300	5.041 (40)	$0.578^{+13}_{-19}$	1.480 (22)
$e_3$	5.25	0.13520	1.9603	8200	5.137 (49)		1.978 (22)
$e_4$	5.20	0.13500	2.0171	7800	4.754 (40)	$0.700^{+12}_{-10}$	1.925 (38)
$e_5$	5.26	0.13450	1.9497	4100	4.708 (52)	$0.783^{+5}_{-5}$	2.406 (27)
$e_6$	5.29	0.13400	1.9192	3900	4.754 (40)	$0.835^{+7}_{-7}$	2.776 (32)

Table 1: The ensembles studied, with measurements made every tenth HMC trajectory. Numbers in italics are preliminary estimates.

ens.	$t_{\text{low}}$	$t_{\text{high}}$	$N_{\text{dof}}$	$^2\text{-dof}$	$Q$	$\hat{m}_t$	$\hat{P}_K$	$\hat{r}_0 \hat{P}_K$
$e_1$	2	4	7	0.485	0.846	0.628 (15)	0.208 (3)	1.085 (17)
$e_2$	2	4	5	0.218	0.955	0.765 (41)	0.228 (6)	1.149 (32)
$e_3$	2	6	9	1.389	0.187	0.683 (24)	0.216 (4)	1.111 (23)
$e_4$	2	5	7	0.292	0.957	0.905 (48)	0.246 (7)	1.171 (33)
$e_5$	2	4	6	0.511	0.801	0.794 (54)	0.232 (8)	1.091 (40)
$e_6$	2	4	5	0.638	0.671	0.832 (35)	0.237 (5)	1.126 (26)

Table 2: Fitting the ground state torelon masses and string tensions.

ens.	$M(t=0)$	$M(t=0)$
$e_1$	0.0016 (60)	0.011 (15)
$e_2$	0.0078 (37)	0.014 (11)
$e_3$	0.0070 (132)	0.0018 (53)
$e_4$	0.0018 (37)	0.0058 (65)
$e_5$	0.0028 (58)	0.014 (11)
$e_6$	0.0001 (58)	0.003 (6)

Table 3: Overlaps between orthogonal torelons and between  $A_1^{++}$  torelon combinations and the scalar glueball.

ens.	$t_{\text{low}}$	$t_{\text{high}}$	$N_{\text{dof}}$	$\chi^2/\text{dof}$	$Q$	$\hat{m}_G(A_1^{++})$
$e_1$	2	4	6	0.352	0.909	0.677 (75)
$e_2$	2	5	8	0.675	0.714	0.628 (30)
$e_3$	2	5	8	0.540	0.827	0.617 (41)
$e_4$	2	4	6	0.923	0.477	0.626 (41)
$e_5$	2	5	8	0.641	0.744	0.654 (30)
$e_6$	2	4	5	1.768	0.116	0.654 (40)

Table 4: Fitting the ground state scalar glueball masses.

ens.	$t_{\text{low}}$	$t_{\text{high}}$	$N_{\text{dof}}$	$\chi^2/\text{dof}$	$Q$	$\hat{m}_G(T_2^{++})$
$e_1$	2	3	3	0.378	0.769	0.88 (8)
$e_2$	2	3	3	0.042	0.989	1.28 (9)
$e_3$	2	3	4	1.651	0.158	1.12 (9)
$e_4$	2	3	4	0.772	0.543	1.33 (9)
$e_5$	2	3	4	0.341	0.850	1.18 (12)
$e_6$	2	3	3	0.399	0.754	1.14 (11)

Table 5: Fitting the ground state tensor glueball masses.

ens.	$t_{\text{low}}$	$t_{\text{high}}$	$N_{\text{dof}}$	$\chi^2/\text{dof}$	$Q$	$\hat{m}_G(A_1^{++})$
$e_1$	2	2	1	0.883	0.347	1.12 (52)
$e_2$	2	2	1	0.312	0.576	1.11 (18)
$e_3$	2	2	1	1.606	0.205	0.94 (23)
$e_4$	1	1	1	1.377	0.241	1.31 (7)
$e_5$	1	1	1	2.751	0.097	1.32 (10)
$e_6$	2	2	1	0.042	0.837	1.17 (32)

Table 6: Fitting the 1<sup>st</sup> excited scalar glueball masses. Numbers in italics are upper bounds from  $t = 1$  only.

ens.	$t_{\text{low}}$	$t_{\text{high}}$	$N_{\text{dof}}$	$\chi^2/\text{dof}$	$Q$	$\hat{m}_G(A_1^+)$
$e_1$	2	2	1	0.281	0.596	1.33 (37)
$e_2$	2	2	1	0.669	0.604	1.34 (28)
$e_3$	2	2	1	0.013	0.909	1.03 (19)
$e_4$	1	1	1	0.009	0.923	1.47 (6)
$e_5$	2	2	1	0.157	0.693	1.24 (54)
$e_6$	2	2	1	0.467	0.495	1.10 (31)

Table 7: Fitting the ground state pseudoscalar glueball masses. Numbers in italics are upper bounds from  $t = 1$  only.

ens.	$t_{\text{low}}$	$t_{\text{high}}$	$N_{\text{dof}}$	$\chi^2/\text{dof}$	$Q$	$\hat{m}_G(T_1^+)$
$e_1$	1	1	1	2.829	0.093	1.44 (7)
$e_2$	2	2	1	0.001	0.982	1.17 (12)
$e_3$	2	2	1	0.023	0.878	1.38 (21)
$e_4$	2	2	1	0.383	0.536	1.68 (22)
$e_5$	1	1	1	1.005	0.316	1.54 (10)
$e_6$	1	1	1	0.010	0.921	1.60 (9)

Table 8: Fitting the ground state vector glueball masses. Numbers in italics are upper bounds from  $t = 1$  only.

ens.	$\hat{m}_G = \hat{P} \hat{K}$	$\hat{r}_0 \hat{m}_G(A_1^{++})$	ratio
$e_1$	3.25 (30)	3.53 (40)	0.96 (12)
$e_2$	2.76 (15)	3.17 (15)	0.86 (5)
$e_3$	2.86 (21)	3.17 (22)	0.86 (7)
$e_4$	2.54 (16)	2.98 (20)	0.81 (6)
$e_5$	2.82 (21)	3.08 (15)	0.84 (5)
$e_6$	2.76 (14)	3.11 (20)	0.85 (6)

Table 9: The scalar glueball masses and their ratios to the quenched mass,  $\hat{r}_0 \hat{m}_G = 3.68$  (8) [3, 13].

ens.	$\hat{m}_G = \hat{P} \hat{K}$	$\hat{r}_0 \hat{m}_G (T_2^{++})$	ratio
e <sub>1</sub>	4.26 (38)	4.62 (41)	0.79 (8)
e <sub>2</sub>	5.60 (37)	6.43 (42)	1.11 (8)
e <sub>3</sub>	5.16 (39)	5.73 (44)	0.98 (8)
e <sub>4</sub>	5.39 (29)	6.32 (40)	1.09 (8)
e <sub>5</sub>	5.10 (50)	5.57 (57)	0.96 (10)
e <sub>6</sub>	4.80 (46)	5.40 (51)	0.93 (9)

Table 10: The tensor glueball masses and their ratios to the quenched mass,  $\hat{r}_0 \hat{m}_G = 5.82$  (14) [3, 13].

ens.	$A_1^{++}$		$A_1^+$		$T_1^+$	
	$\hat{r}_0 \hat{m}_G$	$\hat{m}_G = \hat{P} \hat{K}$	$\hat{r}_0 \hat{m}_G$	$\hat{m}_G = \hat{P} \hat{K}$	$\hat{r}_0 \hat{m}_G$	$\hat{m}_G = \hat{P} \hat{K}$
e <sub>1</sub>	5.9 (2.7)	5.4 (2.5)	6.9 (1.9)	6.4 (1.8)		
e <sub>2</sub>	5.6 (9)	4.85 (84)	6.8 (1.4)	5.9 (1.3)	5.92 (60)	5.15 (53)
e <sub>3</sub>	4.8 (1.2)	4.4 (1.1)	5.3 (1.0)	4.8 (9)	7.1 (1.1)	6.4 (1.0)
e <sub>4</sub>					8.0 (1.0)	6.83 (93)
e <sub>5</sub>			5.9 (2.6)	5.4 (2.4)		
e <sub>6</sub>	5.6 (1.5)	5.0 (1.4)	5.2 (1.5)	4.7 (1.4)		

Table 11: Various other glueball masses, including only estimates from  $t = 2$ .

$\hat{m}^e(t)$		
t	dynamical	quenched
0	0.851 (23)	0.901 (6)
1	0.638 (24)	0.795 (11)
2	0.580 (41)	0.754 (28)
3	0.768 (80)	0.740 (49)

Table 12: The scalar glueball effective mass as a function of  $t$ , comparing the  $P = 0$  values from the e<sub>2</sub> ensemble with quenched calculations at  $\beta = 5.93$ .



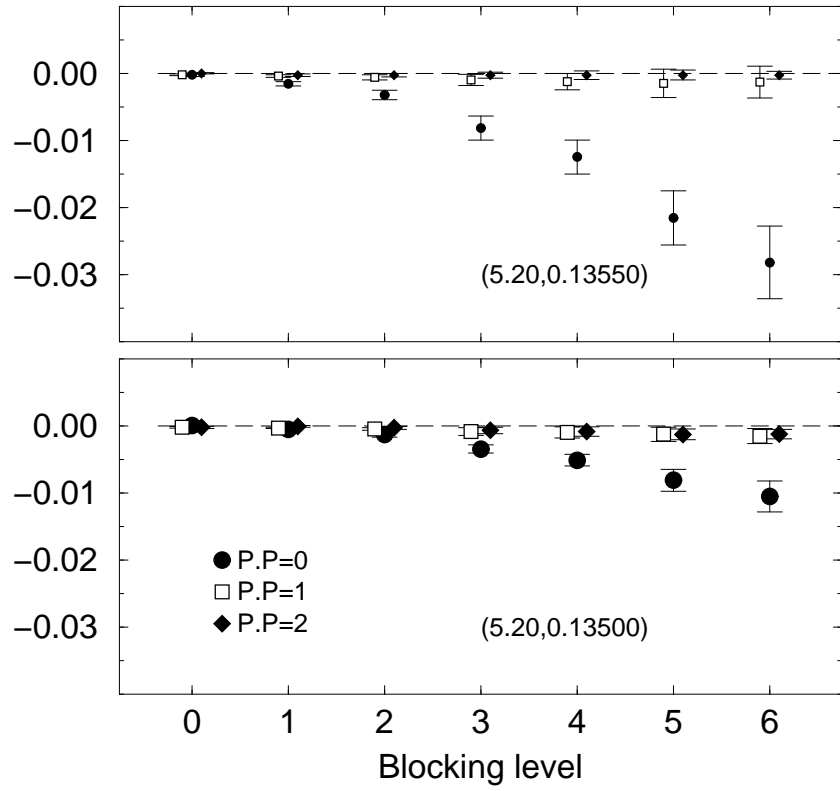


Figure 1: Vacuum expectation values for Polyakov loops at various blocking levels on the  $e_2$  and  $e_4$  ensembles. Plotting point radii are proportional to  $\hat{r}_0\hat{r}$ .

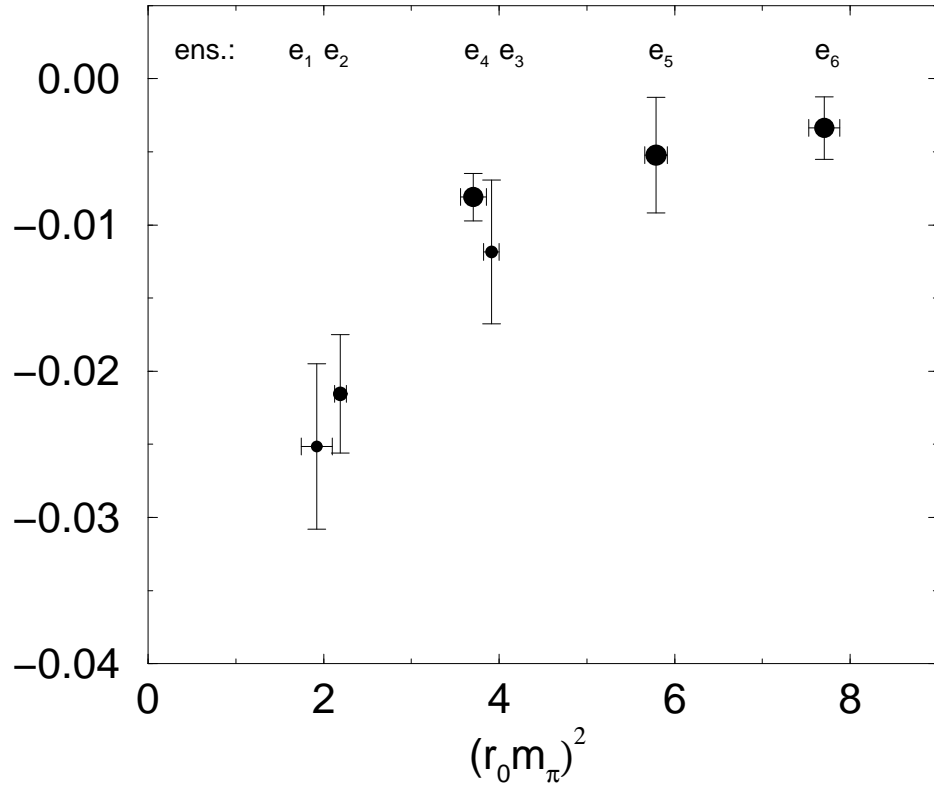


Figure 2: Vacuum expectation values for Polyakov loops at the optimal blocking level (5 in each case) versus the squared pion mass. Plotting point radii are proportional to  $\hat{r}_0^{-1}$ .

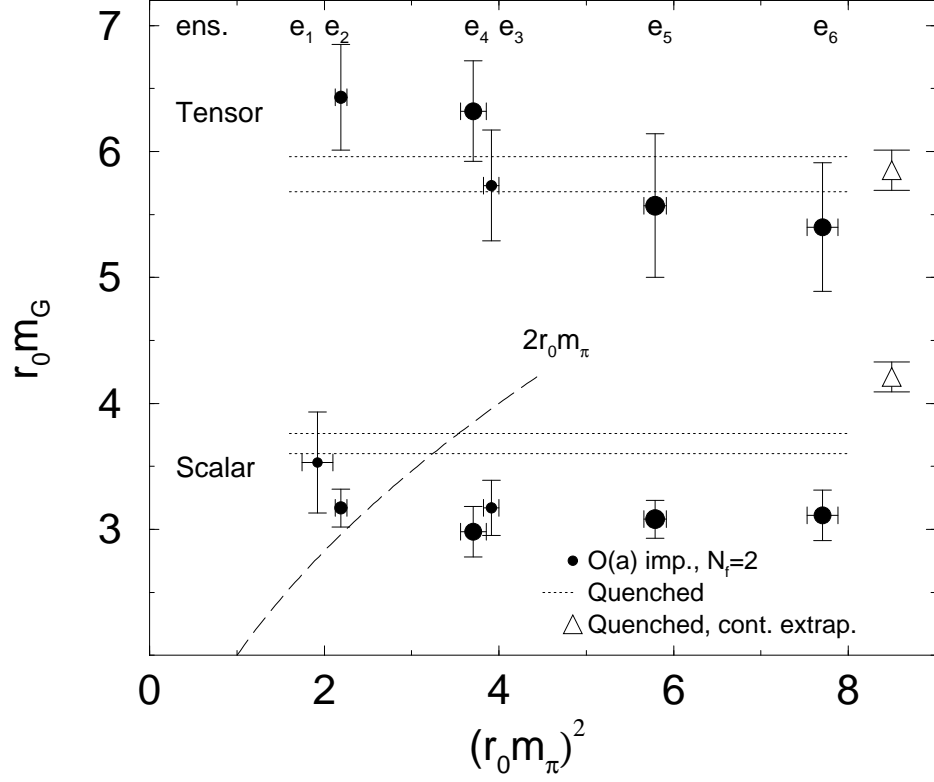


Figure 3: Comparing dynamical and quenched glueball masses. The dashed line is the threshold for decay to  $\pi\pi$ . Dynamical data plotting point radii are proportional to  $\hat{r}_0^{-1}$ . The horizontal bands are the quenched masses at an equivalent lattice spacing,  $\hat{r}_0 = 5.93$  [3, 13]. The quenched continuum limits are from Ref. [2]. N.B.  $\hat{r}_0 m_\pi$  is not applicable to the quenched data.

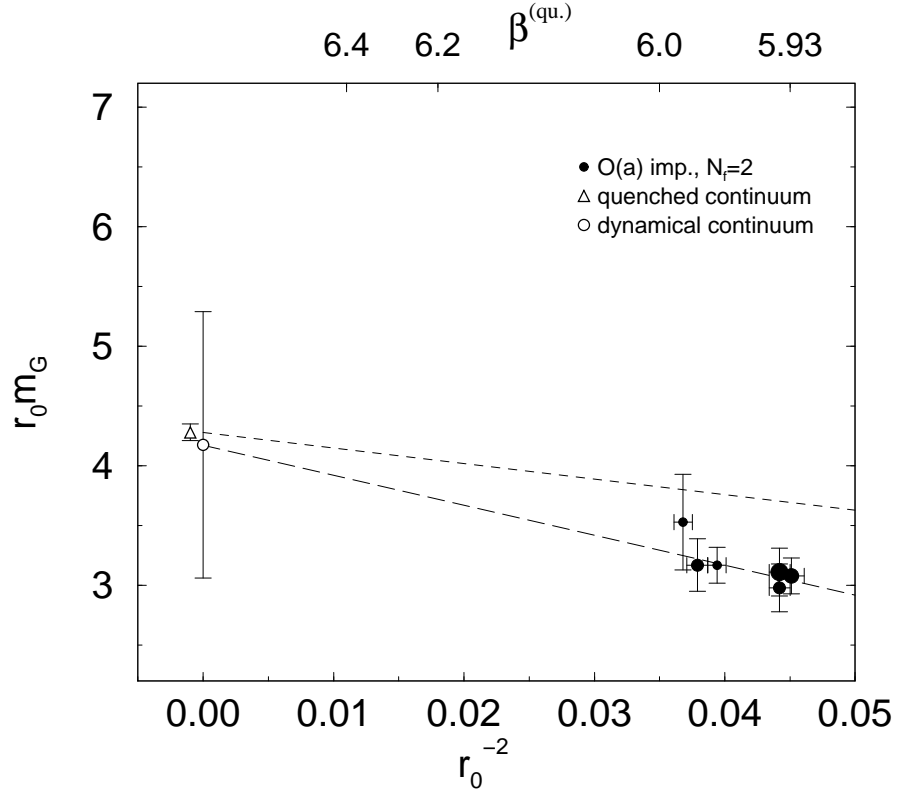


Figure 4: Discretisation effects on scalar glueball mass. Dynamical data plotting point radii are proportional to  $\hat{r}_0 \hat{m}$ . Also shown is the quenched extrapolation, and couplings,  $\beta^{(qu.)}$  yielding these values of  $\hat{r}_0$ .

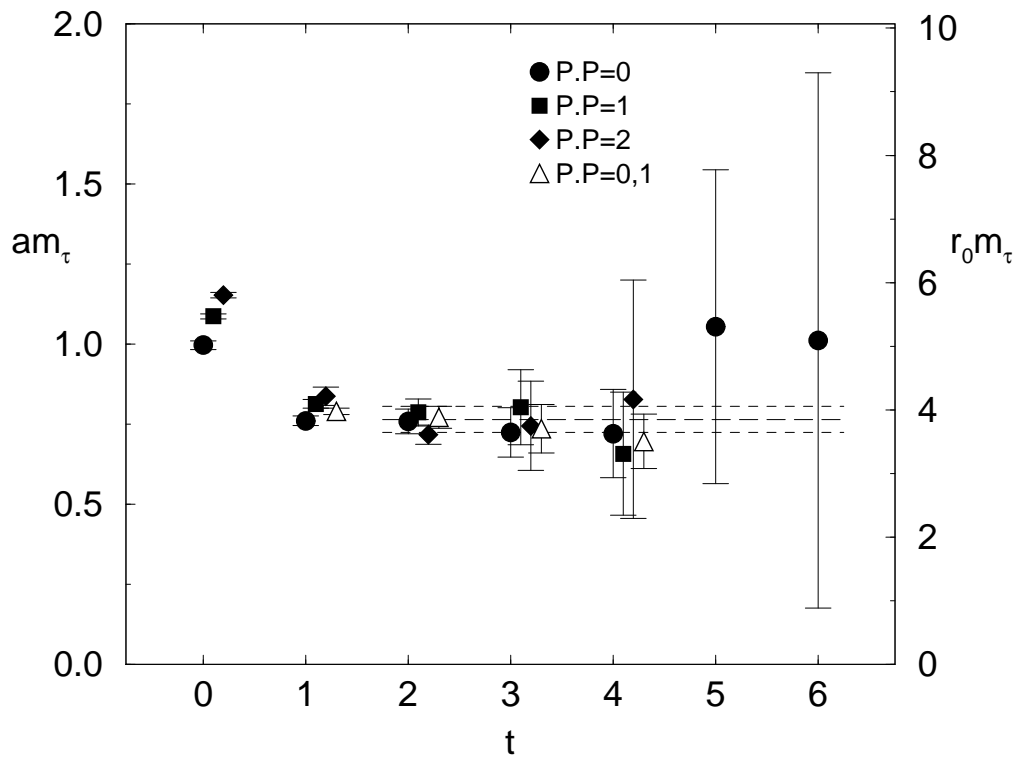


Figure 5: Toren effective mass plot for the  $e_2$  ensemble, with fitted plateau indicated.

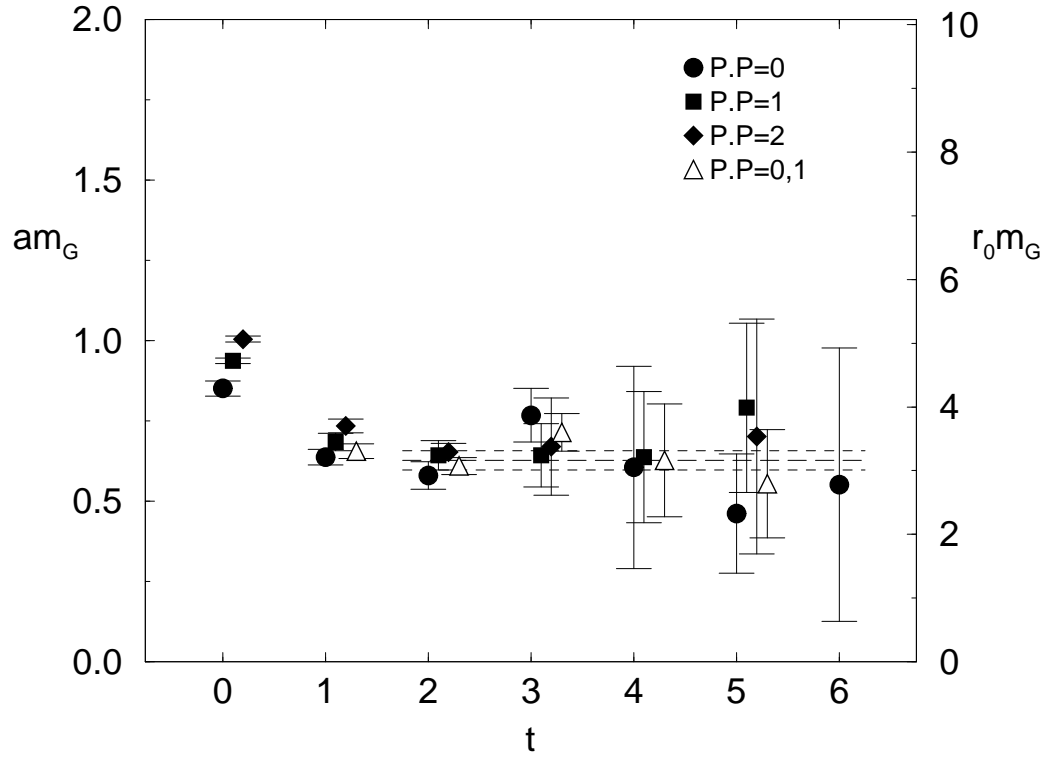


Figure 6: Scalar glueball effective mass plots for the  $e_2$  ensemble, with fitted plateau indicated.

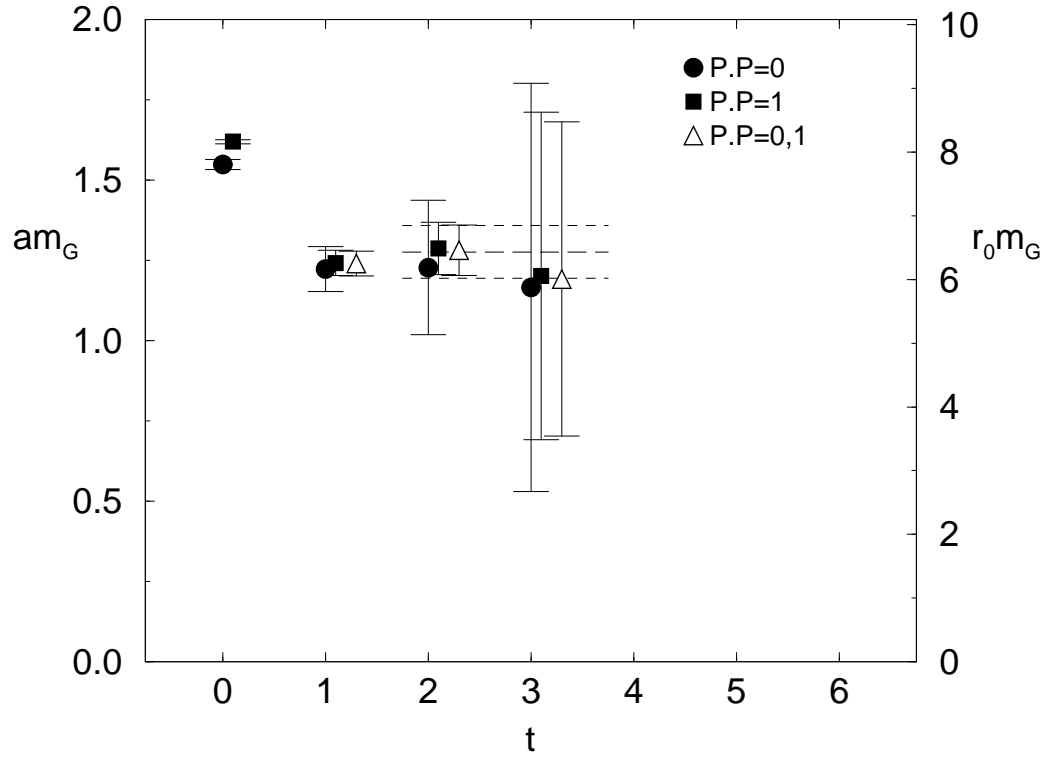


Figure 7: Tensor glueball effective mass plots for the  $e_2$  ensemble, with fitted plateau indicated.

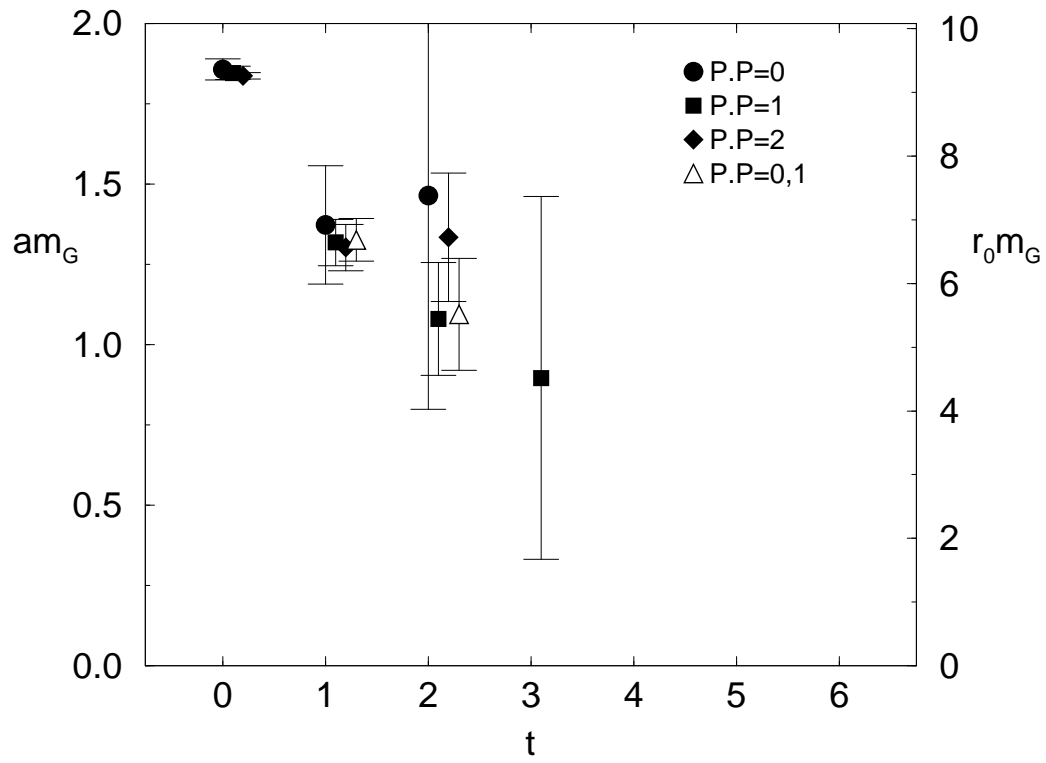


Figure 8: 1<sup>st</sup> excited  $A_1^{++}$  scalar glueball effective mass plots for the  $e_2$  ensemble.



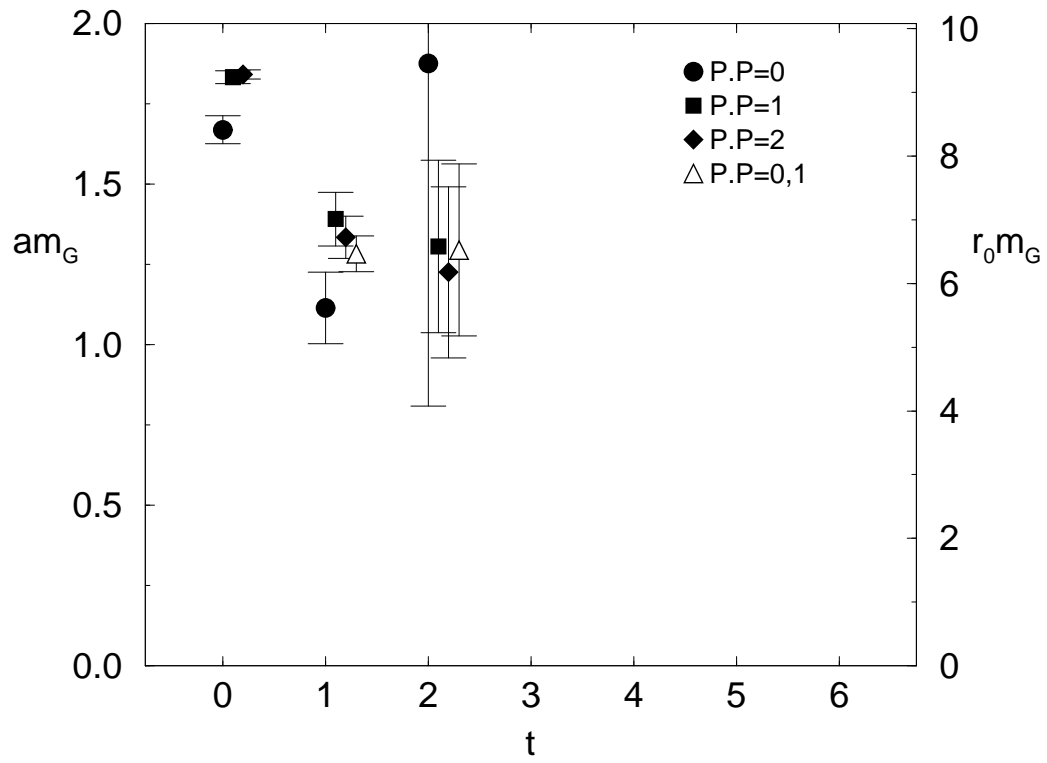


Figure 9:  $A_1^+$  pseudoscalar glueball effective mass plots for the  $e_2$  ensemble.

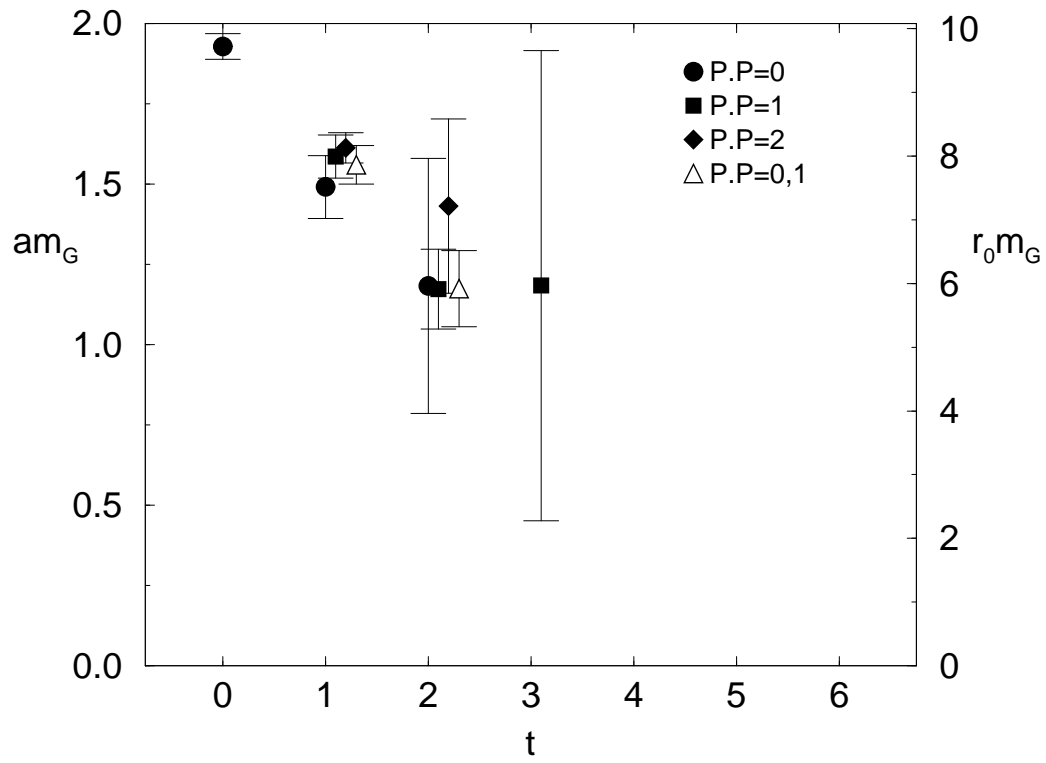


Figure 10:  $T_1^+$  vector glueball effective mass plots for the  $e_2$  ensemble.